

REVIEW

Open Access



# Analysis of the radiated emission of an ECR thruster with magnetic nozzle in terms of its EMC

F. Kiefer<sup>1\*</sup>, K. Keil<sup>1</sup>, K. Holste<sup>1</sup>, P. J. Klar<sup>1</sup> and R. Thüringer<sup>2</sup>

\*Correspondence:  
felix.kiefer@exp1.physik.uni-  
giessen.de

<sup>1</sup> Institute of Experimental  
Physics I, Justus Liebig University,  
Heinrich-Buff-Ring 16, Giessen  
35392, Germany

<sup>2</sup> Center of Competence  
for Nanotechnology  
and Photonics (NanoP), TH  
Mittelhessen - University  
of Applied Sciences,  
Wiesenstraße 14, Giessen 35390,  
Germany

## Abstract

The demand for space propulsion systems is increasing due to the rising number of satellite launches. Electric thrusters gain considerable importance as highly efficient systems in space. As the thrust generation process involves electrically charged particles in motion, ion and plasma thrusters can cause electromagnetic noise, which may interfere with satellite electronics or radio communication. Our objectives are to quantify such emissions and to better understand their origin. We use two facilities to achieve this goal: a semi-anechoic chamber (SAC) with a dedicated vacuum chamber and a mode-tuned vacuum chamber, also known as a reverberation chamber (RVC). Here, we conduct measurements in both facilities on an electron-cyclotron resonance (ECR) thruster with a magnetic nozzle in order to assess its electromagnetic compatibility (EMC). This thruster emits a quasi-neutral plasma plume without requiring an additional neutralizer, thus, is especially suitable for conducting our studies. The thruster in operation acts as an electromagnetic noise source contributing to different frequency ranges. In addition to the excitation frequency band, the data reveals emissions occurring approximately one decade lower in frequency. These emissions depend on propellant mass flow, background pressure and excitation power, i.e., vary with the electron density of the plasma generated inside the ECR thruster. The thruster was characterized following primarily MIL-STD-461G and further ECSS-E-ST-20-07C.

**Keywords:** Electromagnetic interference testing, Plasmas electromagnetic noise, Electric propulsion, Semi-anechoic chamber

## Introduction

The commercial use of space and the increasing integration of the space sector with the traditional economy, known as NewSpace, is progressing rapidly [1–3]. More and more companies from a wide range of industries are using satellite-based technology for a wide variety of applications [4]. Examples include smart agriculture, weather monitoring, remote surgery, the digitalization of industrial production (Industry 4.0) and autonomous driving [3, 4]. Competition between private players is driving innovation that is lowering the barriers to entry into space and reducing the cost of satellites [1]. For example, the cost of putting a satellite into orbit is being significantly reduced by the use of electric space propulsion systems, which use mass-efficient thrusters to enable electric

orbit raising, leading to significant propellant savings. Another trend is the use of small satellites, often in low Earth orbits. This approach is based on technology miniaturization [5].

Space systems can always be classified as complex systems [6]. The functionality and robustness of a satellite, including its functional units, must be proven in a large number of tests on Earth, as it is almost impossible to repair a malfunction in orbit [6]. By accepting a higher risk of failure, development cycles can be shortened to further reduce costs and accelerate the payback of such an investment. Despite this paradigm shift, general requirements such as reliability, robustness and efficiency remain important requirements for mission success and concern not only the propulsion system but also its interaction with other electronic components [2, 3].

Safety requirements—where they exist—are assured by standardized test procedures. However, such test standards are not fully implemented for all components of a satellite. For example, ion thrusters only operate under vacuum conditions and therefore need a special test environment during electromagnetic compatibility (EMC) testing [7]. Test facilities that provide both a vacuum and an EMC test environment are rare. Although the measurement methods used in EMC assessment are based on common standards, they are not construed for EP systems operating in vacuum, but for testing under atmospheric conditions.

It is of particular interest to study the EMC of space systems [6] including electrical propulsion systems in operation [7–9] to reduce the risk of failures of entire satellites or spacecraft systems caused by the propulsion system. EM radiation originating from plasma generation by a thruster or plume extraction can affect sensitive subsystems such as sensors or radio communications by causing unwanted electromagnetic interference (EMI) or changing the subsystems' characteristics [7]. Mission restrictions or failures may occur [6] even if the interference is reversible and only occurs during thruster operation, e.g., attitude control, station keeping or orbit raising. Up to now, in contrast to all other subsystems of a spacecraft, the EMI caused by an operating ion thruster cannot be assessed in a conventional standardized EMC test environment, i.e., specific test facilities are required which enable an operation of the device under test (DUT) or the equipment under test (EUT) in a space-like vacuum environment.

The aim of this study is to estimate the impact of plasma-related effects on the EMI of a spacecraft in case of a specific DUT, an electron cyclotron resonance (ECR) thruster with a magnetic nozzle built by ONERA [10–14], and to distinguish between the plasma-related emissions and those of the electronics required to operate the thruster. For this purpose, we measure the emission spectrum of the same operating thruster using two different dedicated setups. One is a vacuum reverberation chamber (RVC) [15], and the other a semi-anechoic chamber (SAC) connected to a vacuum system [16].

The used ECR thruster with a magnetic nozzle was one of the prototypes of the MINOTOR project and was developed and lent to us by ONERA. It is further described in [10–14]. This type of thruster is particularly suited for establishing procedures for studying EM effects of electric thrusters in operation. The reasons are manifold. First, it emits a quasi-neutral plasma. Therefore, the use of an additional neutralizer, whose power electronics may also interfere with the operation of the thruster itself or with other components of the system, is not required. Second, because of the absence of an

additional neutralizer, the rotational symmetry of the ECR thruster about the thrust direction implies that its EM emission characteristics possesses the same symmetry. The high symmetry simplifies a complete assessment of the EM characteristics of the thruster. Third, the microwave frequency of  $f_x = 2.45$  GHz used for exciting the plasma of the ECR thruster during operation is quite high compared to those, for example, used in radio frequency ion thrusters (RIT), which typically operate in the lower MHz or upper kHz range [2]. According to the standards, the radiated EMI should be measured in a frequency range from at least 30 MHz to 18 GHz [17, 18]. Thus, an excitation frequency of  $f_x = 2.45$  GHz means that the most only six harmonics are observable in the frequency range of interest. As a consequence, the effects of the excitation signal should be well distinguishable from superimposed plasma-related effects caused by the excitation. In contrast, RIT operation in the MHz range can have hundreds of harmonics superimposed on the plasma-related emission. These advantages make the ECR thruster ideally suited for investigating the electromagnetic emissions of a plasma-based ion source in operation.

This paper is organized as follows: “[Experimental approach](#)” section outlines the experimental methods used, covering the SAC and the RVC facility, the selected thruster, as well as data management procedures. “[Measurement results](#)” section presents and compares EMI data of the ECR thruster obtained in both facilities using different measurement approaches. We systematically studied the EM emission of the thruster in dependence on the three main operational parameters, the propellant mass flow  $Q$ , the excitation power  $P_x$  and excitation frequency  $f_x$ . In “[Conclusion](#)” section, we conclude by providing a brief summary of our findings and an outlook on future work needed to better understand the EM behavior of electric thrusters.

### **Experimental approach**

Standards used in the qualification of equipment for space applications are, for example, the MIL-STD [17] or the ECSS-E-ST [18]. In these documents, EM assessment is divided into subsections, primarily distinguishing between conducted and radiated disturbances, which are secondarily specified by susceptibility and emission, also called interference. By means of susceptibility measurements, a DUT, in our case the electric thruster with or without corresponding electronics, has to prove that it is not susceptible to external EM disturbances. Conversely, emission tests are performed to quantify the EM fields emitted by the DUT to potential receivers. Both tests can be either performed in conducted mode, which primarily probes the lower frequency ranges down to kHz, or in radiated mode, which typically addresses the MHz frequency range and above. Since a plasma plume of an ECR thruster consists of charged particles that are not intentionally associated with the spacecraft, we focus on the radiated emissions (RE) from the operating electric thruster. In order to obtain data that meets the requirements of the above standards, we use the RVC test facility and the SAC test facility described in [15, 16], respectively. More details about the measurement approach based on the SAC test facility are given in Fig. 1. Basically, it can be compared to the one employed at The Aerospace Corporation (USA) [19, 20], at Aerospazio Tecnologie S.r.l. (Italy) [21, 22] and at Moscow Aviation Institute (Russia) [23–26].

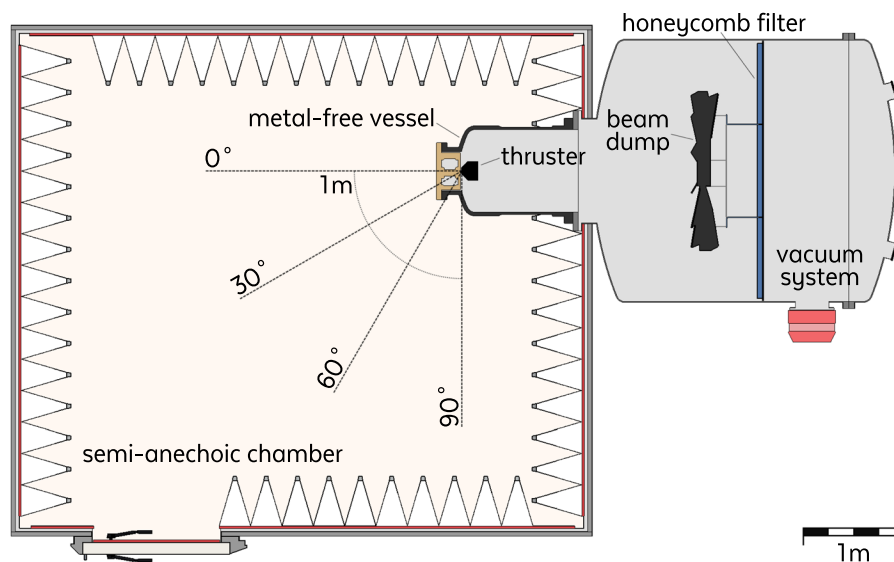


**Fig. 1** Schematic layout of the facility consisting of the SAC with pyramidal absorbers on ferrite-covered walls, references to the antenna positions used to measure RE, the inner EM transparent vessel surrounding the mounted thruster. The thruster expels its plasma plume into the outer vacuum vessel with the beam dump, honeycomb filter, and vacuum pump system

The main component of this facility is a SAC that was designed to meet MIL-STD-461G (MIL) and ECSS-E-ST-20-07C (ECSS). It consists of a metal enclosure that shields the interior from ambient EM noise caused by radio stations or communications infrastructure etc. To allow for a free-space-like propagation of EM waves emitted by the DUT inside the SAC, internal reflections of EM waves from the walls need to be avoided. This is achieved by pyramidal absorbers mounted on the walls and the ceiling. As there are no absorbers on the floor, the room is semi-anechoic rather than completely anechoic. To further improve the attenuation of the walls, ferrite plates are placed between the absorber structure and the conductive enclosure. A vacuum chamber is attached to the SAC, as this standardized facility alone does not provide the vacuum conditions required for the operation of electric propulsion (EP) systems. It consists of a large metal vessel placed behind an opening in the shielding of the SAC and is attached to its conductive walls. A metal-free cylinder made of glass reinforced plastic (GRP) is connected to the metal vessel and extends into the SAC. Its epoxy resin can stand temperatures of up to 130 °C and is transparent for EM waves. The vacuum chamber consisting of metal vessel and GRP cylinder is equipped with a pumping system. The thruster is mounted in the GRP cylinder in such a way that the expelled plasma plume hits the beam dump made of graphite, which reduces sputtering effects [27, 28]. The internal diameter of the GRP cylinder is 0.8 m whose cylindrical length is below 1.2 m from the thrusters mounting flange towards the beam dump and is therefore primarily suitable for relatively small DUT. However, the opening in the SAC wall allows to mount a cylinder or cone with a flange diameter of up to 1 m in the SAC wall.

The pumping infrastructure comprises a turbomolecular pump with a  $N_2$  pumping speed of up to 4300 l/s. It is complemented by an additional cryogenic vacuum pump, which has been put into service at the end of our test series. The achieved background

pressures inside the SAC as well as RVC facility in dependence on the propellant mass flow used are summarized in Table 1. A circular honeycomb filter with a diameter of about 2 m and 60 mm in depth, which is placed behind the beam dump, divides the vacuum vessel into two compartments. Thus, it separates the pumping system from the thruster. The honeycomb structure behaves like a conducting wall and shields EM waves. Furthermore, it exerts such a low flow resistance on the vacuum system that we were not able to measure any significant pressure difference at mass flows of up to  $Q=5$  sccm propellant flow. It damps EM noise coming from the pumps below the measurement sensitivity up to at least 40 GHz. Therefore, the measurements of background noise described in [7] could be neglected in our measurements, since background noise should be reduced far below the noise floor of the measurement system.

The cylindrical GRP vessel inside the SAC must be metal-free so that the EM fields and waves generated by the thruster and its plasma can pass through it with negligible absorption losses and be measured by suitable antennas inside the facility. To identify the spatial direction in which a DUT exhibits the strongest EM emission, DUT and antenna arrangement should ideally be freely rotatable about each other. However, as the thruster’s plume needs to be directed towards the beam dump, the thruster can at most be rotated about one axis, so that two degrees of freedom are lost. If instead the antenna is rotated in a quadrant about the DUT, all solid angles can be captured that lie on the hemisphere opposite the plume direction. Any thruster that has a rotational symmetry about the plume direction (which is the case for most common thruster designs) should exhibit an EM emission of rotational symmetry about the plume direction. If a neutralizer is employed, the neutralizer may break the rotational symmetry of the EM emission of the thruster system. However, the plasma plume of the ECR thruster studied is quasi-neutral. Therefore, it does not require a neutralizer and the assumption of its EM emission being symmetric about the plume direction should be valid. For this reason, we believe that the rotation of the antenna about the DUT is more relevant for the investigation of the EM emissions of the plasma-related emission of the thruster than the rotation of the ECR thruster about the plume direction. We recorded data at the four discrete antenna positions, at a distance of 1 m from the thruster mounting flange, shown in Fig. 1. The rotation axis of the antenna is centered close to the mounting flange rather than at the exit plane of the thruster. The reasons are, first, the same position can be used for different thrusters as DUT and, second, reproducibility of the antenna positions is facilitated.

**Table 1** Typical background pressures in vacuum vessels of EMC test facilities SAC and RVC obtained using a turbomolecular pumping system or, if available, turbomolecular and cryogenic pumping system for given propellant mass flows  $Q$

Q inlet	SAC		RVC
	turbo	turbo + cryo	turbo
0 sccm	$\approx 3 \times 10^{-7}$ mbar	$\approx 4 \times 10^{-8}$ mbar	$\approx 5 \times 10^{-7}$ mbar
1 sccm Xe	$2.2 \times 10^{-5}$ mbar	$3.6 \times 10^{-6}$ mbar	$3.3 \times 10^{-5}$ mbar
1.5 sccm Xe	$3.2 \times 10^{-5}$ mbar		$5.3 \times 10^{-5}$ mbar
2 sccm Xe	$4.3 \times 10^{-5}$ mbar		$6.9 \times 10^{-5}$ mbar

In each position, two linear sweeps were performed over the frequency range from 30 MHz to 18 GHz, one for horizontal (H) and the other for vertical (V) antenna polarization, as demanded in MIL [17] and ECSS [18]. Most standards, such as ECSS [18], require 30 MHz as lower limit for radiated emission measurements. However, MIL [17] demands measurements down to 10 kHz for space applications. This requires the use of an additional rod antenna. Since such an antenna was not available, we focused on measurements above 30 MHz in accordance with ECSS [18]. At each frequency point  $f$ , the measuring receiver records the amplitude data  $A(f)$  for the recommended detector, which in our case was a maximum peak (max.-peak) detector. Thus, a complete data set contains several sweeps  $A_{p,a}(f)$ , where the subscript  $p$  represents the antenna polarization H or V and  $a$  denotes the angular position 0, 30, 60 or 90 degrees. The angular resolution can be further increased, if a turntable is used to rotate the antenna inside the SAC. We used an ESW26 measuring receiver from Rohde & Schwarz, which also supplied the corresponding software EMC32 for the acquisition of  $A_{p,a}(f)$ . In a second step, the data sets obtained are reduced according to

$$A_{\max}(f) = \max\{A_{p,a}(f) | p \in \{H, V\}, a \in \{0, \dots, 90\}\} \quad (1)$$

which represents a reduction of the highest field strength values at each  $f$  to a single frequency sweep  $A_{\max}(f)$ . If the frequency-dependent transfer function of the antenna including the connecting cable is known, the electric field strength at the antenna can be reconstructed from this data set.

Any manual placement of an antenna is associated with a certain degree of uncertainty in position and orientation. Three antennas are required to cover the broadband spectrum from 30 MHz to 18 GHz [17, 18], four if the spectrum is extended to 40 GHz, and a fifth if it is extended down to 10 kHz [17]. Therefore, several antenna rearrangements and polarization changes are required for a full-range investigation. Reducing the number of rearrangements can indirectly reduce the adjustment uncertainties and additionally speed up the measurement cycles, which in turn should reduce effects of drift in the operating parameters of the DUT.

Our antenna arrangement consisted of two antennas only. First, a logarithmic-periodic antenna was used between 30 and 700 MHz (although an additional biconical antenna should be used below 200 MHz). Second, a logarithmic-periodic antenna was also used above 700 MHz. It should be noted that MIL [17] and ECSS [18] recommend a horn antenna above 1 GHz instead. Unfortunately, logarithmic-periodic antennas are not recommended by MIL [17] but other antennas were not available at the beginning of our study which is why those antennas were chosen. The non-conformal transition frequency of 700 MHz was chosen because the preamplifier used can improve the sensitivity of the second antenna even below the required transition at 1 GHz. According to MIL [17], the measurement bandwidth (BW) should be 100 kHz below and 1 MHz above the antenna transition at 1 GHz, using a linear sweep with half the BW step size. However, even though we chose to use a reduced crossover at 700 MHz, the measurement bandwidth was changed at 1 GHz. Covering the entire frequency range from 30 MHz to 18 GHz with two antennas only, allowed us to use a tripod to mount the two antennas and to simultaneously align them with the DUT. The arrangement used, shown in Fig. 2a, with only two instead of three antennas, is not in full accordance with the

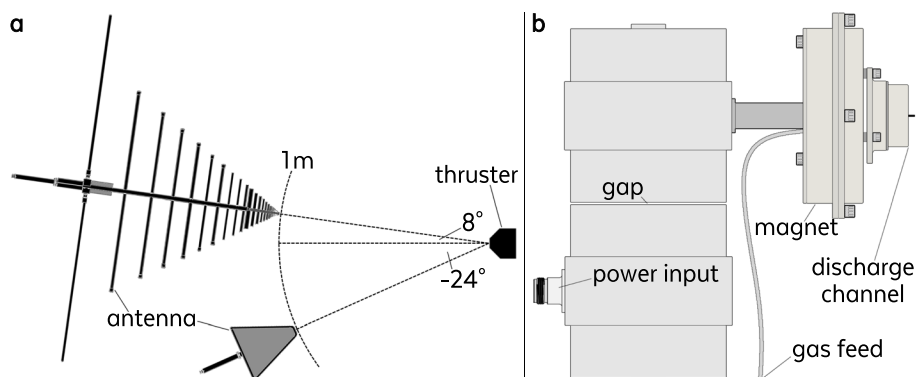


**Fig. 2** Antenna setup and DUT, **a** side view of antenna arrangement for vertical polarization to measure 30 MHz to 18 GHz at 1 m tip to thruster and **b** ECR thruster illustration with gapped waveguide to isolate thruster (DUT) against ground

named standards. Both antennas were mounted comparatively close to each other and, thus, may influence each other's antenna factors, especially in the lower frequency range. However, the main advantages of this arrangement are faster measurements, which reduce thermal drifts, and increase reproducibility of the setup. Furthermore, in position  $90^\circ$  the antennas are located relatively close to the absorbers due to the dimensions of the GRP vessel. Increasing the length of the GRP vessel and using smaller absorbers in this area may overcome this issue.

The ECR thruster used as the plasma source, which was one of the prototypes developed by ONERA during the course of the MINOTOR project and was lent for our study, is described in detail in [10–14]. Its magnet provides a flux density of 0.0875 T to achieve ECR excitation at  $f_x = 2.45$  GHz. The ECR thruster is shown schematically in Fig. 2b. It consists of a waveguide through which the applied radio frequency (RF) power is transmitted. Its symmetrical structure is separated by an air gap of  $< 1$  mm, which avoids mechanical interaction of the RF feed line during measurements on a thrust balance [29]. Another function of the gap is to isolate the thruster from ground, allowing simplified measurement of the thruster potential with respect to the vacuum chamber. As a mechanical isolation of the supply line is not a prerequisite for EMC measurements, the gap was sealed using a combination of insulating and conductive tape. This was realized in such way, that the thruster is on floating potential whereby the gap is almost RF closed for the operating frequency. The sealing avoids EM radiation of the RF excitation to leak through the gap and to interfere with the radiated EM emissions of the operating thruster.

The ECR thruster was operated using operating parameters as close as possible to those given in [10]. Xenon was used as propellant and the propellant mass flow was varied in the range of  $Q = 0.7$  sccm to 2 sccm. Three different excitation powers  $P_{f-r} = 20$  W, 25 W, and 30 W were initially studied, but since their influence on the EMI spectrum appears to be small, only data for  $P_x = 10$  W (corresponding to  $P_{f-r} = 20$  W) are presented here. The plasma density of  $n_e \approx 1 \times 10^{15} \text{ m}^{-3}$  at  $Q = 1$  sccm and  $P_x = 15$  W at a distance of 11 cm from the thruster exit plane was determined using Langmuir probe measurements as recommended in [30]. The value is in an expected range considering that it was measured at a background pressure which was an order

of magnitude higher [10]. It should be noted that we distinguish between simplified excitation power  $P_{f-r}$  and corrected excitation power  $P_x$ . The former is defined as

$$P_{f-r} = P_f - P_r \quad (2)$$

where  $P_f$  represents the forward power and  $P_r$  the reflected power measured by power sensors via a directional coupler in between the RF generator and the thruster. To obtain the corrected excitation power  $P_x$ , we also have to take into account the total cable attenuation  $A_c$  of the line section between the directional coupler and the waveguide at the thruster yielding

$$P_x = P_f^* - P_r^* = (P_f - A_c) - (P_r + A_c) \quad (3)$$

We used Huber + Suhner SF104 and SF106 RF cables with an attenuation of about 0.34 dB/m, Cellflex LCF 12–50 with an attenuation of about 0.12 dB/m at 2.4 GHz, and comparable types. The attenuation  $A_c$  was determined for each setup, including all connectors, adapters and feedthroughs, and the measured  $P_x$  values were corrected accordingly using Eq. (3). For our setups, the correlation between the two quantities was approximately  $P_x \approx \frac{1}{2} P_{f-r}$ , i.e.,  $A_c \approx 1.5$  dB, since our feeding line was at least 4 m in length. The power values given in [10–14] were corrected in a similar fashion. In the context of our measurements, lower  $P_x$  values were chosen because a less powerful generator was used, providing calibrated power measurement capabilities.

There are no absorbers on the ground of a SAC. Thus, in contrast to a full anechoic system, the reflections from the ground of the SAC can alter the measurement results compared to the free-space situation, since two-way propagation reflections can lead to constructive or destructive interference at the antenna. The IEC61000-04–21 standard provides formulas for estimating the maximum change in amplitude  $g_{\max,p}(f)$  for each polarization  $p$  caused by such ground reflections [31]. Applying Eq. (1), the influence of  $g_{\max,p}(f)$  on the measurement results in the SAC is combined and can be estimated by

$$\widehat{g}_{\max}(f) = \max\{g_{\max,p}(f) | p \in \{H, V\}\} \quad (4)$$

The influence of  $\widehat{g}_{\max}(f)$  for the antenna arrangement shown in Fig. 2a is plotted in Fig. 3 along with  $g_{\max,H}(f)$  and  $g_{\max,V}(f)$  which serves as reference. If relative values in dB are used for both  $\widehat{g}_{\max}(f)$  and the measured values, the ground reflection is corrected by subtracting  $\widehat{g}_{\max}(f)$  from the measured data set.

In addition to EM radiative measurements using the SAC test facility as described above, we also performed corresponding measurements using our RVC test facility. The measurement procedures using the RVC test facility are described in detail in [15]. In brief, its principle of operation can be summarized as follows: The DUT is operated in a metallic vacuum chamber which also acts as a cavity resonator for electromagnetic modes. Stirrers in the RVC detune its resonance and discrete mode distribution such that a quasi-continuous spectrum can be investigated. This operating principle provides the radiated power spectrum of a DUT integrated over all solid angles, especially, if the DUT acts as a periodic emitter. The power spectrum is converted into a field strength as it would be radiated by an antenna and then measured

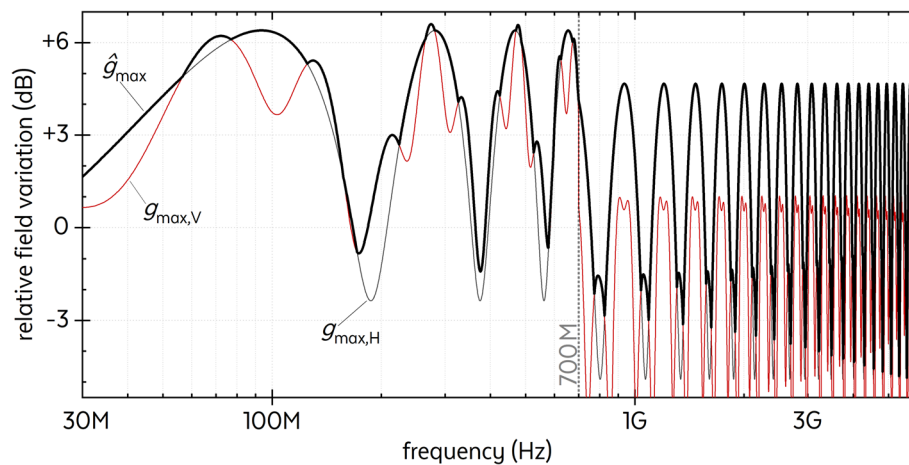


**Fig. 3** Potential influence of ground reflections on results of field measurements in the SAC, estimated according to IEC61000-04-21 for H and V polarization plotted as  $g_{\max,H}$  and  $g_{\max,V}$  as well as  $\hat{g}_{\max}$  in bold line for the deployed antenna arrangement

at a defined distance in the SAC test facility, e.g., 1 m to comply with MIL [17] or ECSS [18] setups. We corrected all our RVC measurements accordingly to be able to compare those with the SAC measurements. The RVC approach can then be used for pre-compliance emission measurements above its low cutoff frequency which is  $f_{\min} \approx 500$  MHz in our case. However, our facility provides additional emission data down to 300 MHz. This low-frequency data does not comply with the underlying IEC61000 standard and also has a lower measurement gain [15], but still is shown for comparison in what follows. In both facilities, a max-peak detector was used for data acquisition.

### Measurement results

The measurement results of the ECR thruster driven at  $f_x = 2.45$  GHz with  $Q = 1$  sccm and  $P_x = 10$  W are shown in Fig. 4a. Radiated emission data was collected based on MIL [17] section RE102 which meets ECSS [18] section A.9 [32] and shows significant peaks at  $f_x$  and its harmonics as well as broadband emission below approximately 300 MHz. The insets 4b and c show the highlighted sections of those results corrected for  $\hat{g}_{\max}$ . In addition, the associated noise plots are also shown in light colors, representing the sensitivity limit of the measurement system that can be observed for selected measurement parameters in the respective facility. We supply the limit lines for MIL [17] and ECSS [18], even though we cannot use them to evaluate whether the thruster complies with those standards. The reason is that different modifications compared to the standards, e.g., antenna arrangement, were utilized and the thruster was operated at reduced power only. Additionally, the MIL [17] standard is usually not applied directly, but in a form such as the MSFC-SPEC-521 [33] or GSFC-STD-7000A [34] standard. For example, the MSFC-SPEC-521 is tailoring the MIL specifications in order to prevent over-specification of requirements and still maintain EMC [33].

The discontinuous shape of the noise plots is characteristic because various aspects have to be taken into account which are discussed in what follows. The abrupt jump in

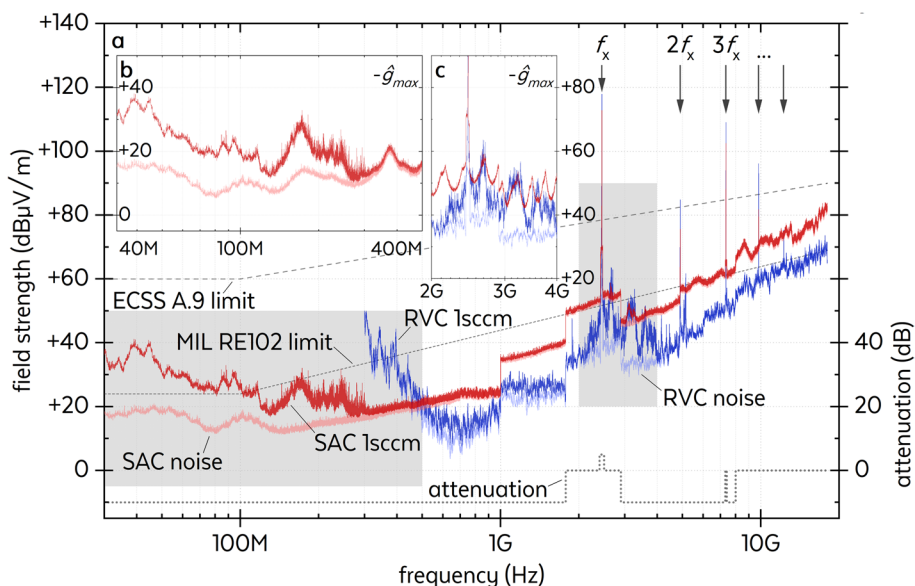


**Fig. 4** Electromagnetic radiated emissions of the ECR thruster operated with  $P_x = 10$  W excitation at  $f_x = 2.45$  GHz and  $Q = 1$  sccm xenon propellant flow measured by max-peak detector in SAC and RVC at 1 m antenna distance with corresponding noise floors and added attenuations. **a** shows the broadband result measured according to MIL-STD and ECSS-E-ST and **b** and **c** show different sections of this result corrected for  $\hat{g}_{max}$

the measured curves at 1 GHz is a consequence of the bandwidth parameter change recommended by MIL [17] and ECSS [18]. The abrupt jumps at 1.8 GHz and 2.4 GHz and the subsequent plateaus up to 2.5 GHz and 3 GHz, respectively, which are particularly visible in the SAC data, are the result of programmable attenuations for the corresponding discrete frequency bands. These narrowband attenuations were needed to prevent the measurement receiver from saturation at high DUT emissions. The dashed lines in Fig. 4a illustrate the programmed attenuations. Values below zero represent activation of the ESW26 measurement receiver’s internal preamplifier which reduces the noise floor to lower values, which means higher measuring sensitivity. Since this amplifier has an upper cut-off frequency at 8 GHz, an abrupt jump can be observed at that frequency in the SAC data. The reason is that the actual gain of this amplifier is calibrated internally. It appears to be nonlinear, so the amplitude of the described jump does not match the amplitude in the attenuations shown. It should be noted that the programmed attenuations used for the measurements inside the RVC facility were optimized for the thruster operating point discussed. The same attenuations were also used in the measurements inside the SAC test facility for comparability. The attenuations were chosen such that the measurement receiver does not exceed its input limit regardless of the DUT operating point.

The overall increasing trend in the data of EM emission vs frequency shown in Fig. 4 is a result of Maxwell’s law. Antenna factor tables typically enhance these nonlinearities. The reason is a higher frequency of the constant system noise measured in dBm results in increasing magnitudes when converted to field values such as dBμV/m. For a constant noise power, the field values will increase by 20 dB per decade because this transformation is proportional to  $f$ . Furthermore, the cable attenuation increases at higher

frequencies. Both effects together account for the observed trend. The attenuation may be reduced by using shorter cables. However, this would affect the overall setup, as the antennas in the SAC require relatively long connections that they can be moved about the GRP cylinder on a circular arc. In principle, a pre-amplifier attached to the antenna may be used as another option. However, such a broadband amplifier cannot be employed in case of DUT with high EM excitation power in a narrow frequency band, as such a high input signal may overload the output emission signal, no matter how narrow the latter is. This is the case with the ECR thruster as DUT, which is operated with  $f_x = 2.45$  GHz excitation.

A preliminary conclusion is that all nonlinearities appearing in the noise plots, even without an emitting DUT, are a consequence of fluctuations in the calibration curves used to correct the raw values at the end of the measurement chain for the system response. In addition to the attenuations or gains mentioned above, these corrections account for the antenna factors and the system gain of the RVC.

We now turn to the results of the DUT's radiated emission, shown in Fig. 4. Readings of the field strengths were calculated as commonly performed in such measurements. However, absolute values captured with our setups may not represent the field strengths a DUT emits in its far field. The reasons for that are different assumptions of field uniformities in the setups used. These are, e.g., the calculation of the field strength in the RVC and the measurement of the field strength inside the SAC at 1 m distance, which is in the near field of the DUT below 700 MHz for a broadband spectrum in case of the antenna used [35]. For this reason, we focus on qualitative effects that can be observed in our data, rather than a quantitative interpretation of the measured values.

As expected, the dominant frequency peak at  $f_x = 2.45$  GHz and its associated harmonics, marked by arrows, can be observed. Sidebands above  $f_x$  appear to be an effect of the generation and transmission of the excitation signal. Some of these sidebands appear to have a harmonic band at  $2f_x$ , supporting the assumption that they are generator emissions. However, even though we cannot apply the limit lines, our data of the emission behavior, apart from that at the excitation frequency and its harmonics, seems to be in accordance with ECSS [18] limit for radiated emission while operating the DUT at the chosen parameters. Exceeding the limits at the excitation frequency and its harmonics is permissible, as the ECR thruster can be regarded as a radio-technical device and these frequencies are required for its operation.

In order to assess the influence of the excitation generator, we collected data sets at high resolution, which are shown in Fig. 5. In graph 5a, we focus on the side bands of the peak corresponding to the excitation frequency  $f_x$  already indicated in Fig. 4. In addition to the noise floor, measurements at  $Q = 0$  sccm serve as a reference to determine the emissions of the generator without plasma. These measurements were conducted at  $P_x = 2$  W, which should correspond to an attenuation of 14 dB $\mu$ V/m on the logarithmic scale. However, the peak corresponding to  $f_x$  at  $Q = 0$  sccm and  $P_x = 2$  W without plasma has the same amplitude than that recorded with plasma at  $Q = 1$  sccm and  $P_x = 10$  W. A possible reason is that in the latter case about 80 % of the excitation power is transferred to the ignited plasma, which reduces the peak at  $Q = 1$  sccm accordingly. This correlates with our observation that excitation with  $P_x = 10$  W at  $Q = 0$  sccm (without plasma)

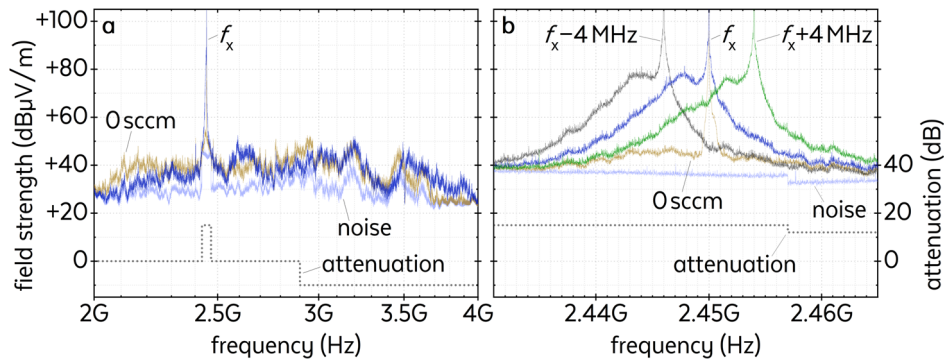


**Fig. 5** Electromagnetic emission spectra of the ECR thruster operating at  $Q=1$  sccm xenon propellant and  $P_x=10$  W in the RVC test facility. The spectra are measured by a max.-peak detector and correspond to 1 m antenna distance. **a** of side bands of the peak corresponding to the excitation frequency  $f_x=2.45$  GHz in a larger range from 2 to 4 GHz. **b** in the vicinity of the peak corresponding to the excitation frequency  $f_x$  for three different values  $f_x=2.45$  GHz, and  $2.45$  GHz  $\pm$  4 MHz. In both graphs we also show the curves representing noise floor, added attenuation, and an excitation reference without plasma at  $Q=0$  sccm and  $P_x=2$  W at  $f_x=2.45$  GHz

leads to overloading of the measurement receiver, so  $P_x$  had to be reduced in order to obtain reference data with the same attenuation settings for comparing the plots.

The aforementioned sidebands are not as clearly visible in Fig. 5a as in Fig. 4. The main reason is the reduced measurement BW, which is set to twice the step size in the high-resolution scan. The noise and emission levels seem to increase with the BW, since EMC measurements are not normalized for the BW used. As a result, the sidebands in the vicinity of  $f_x$  have a higher amplitude in Fig. 4 and are less pronounced in the high resolution measurement depicted in Fig. 5. We assume that the side bands are mainly due to generator effects because the EM emissions without plasma in Fig. 5a are at some frequencies higher than the corresponding measured values with plasma and show no clear trend.

A plasma-related emission is clearly visible only in the vicinity of  $f_x$ , which can be seen in Fig. 5b, when zooming in further. It consists of a well-defined Gaussian band overlapping with the sharp peak at  $f_x=2.45$  GHz. The maximum of the Gaussian band is located at a lower frequency than the excitation frequency  $f_x$ . When tuning the excitation frequency, the Gaussian band follows the frequency shift, as can be seen in the measured curves plotted in blue and ocher where the ECR thruster is excited with  $f_x=2.446$  GHz and 2.454 GHz, respectively. On the basis of the comparison with the EM emission spectra of the ECR thruster obtained without plasma where the Gaussian-type band is not observed, we believe that this feature is not a generator effect. The origin of this effect could be the frequency shift that occurs for damped oscillators in the regime of weak damping [36] given by

$$\omega' = \omega_0 \sqrt{1 - \frac{1}{4 q_s^2}} \quad (5)$$

The quality of the oscillating system is expressed by the quality factor  $q_s$ . The lower the value of  $q_s$ , the more the fundamental oscillation of the system is shifted to lower frequencies. Since an ignited plasma absorbs energy from the  $f_x$  excitation, the plasma

can be considered as the load of the  $f_x$  oscillating ECR thruster system, thus reducing  $q_s$ . It is expected that the reduced  $q_s$  of the system will be accompanied by a broadening of the distribution of excited oscillations, since a system is generally capable of operating over a wider bandwidth as  $q_s$  decreases. All three curves measured for different excitation frequencies  $f_x$  and ignited plasma exhibit a secondary maximum just below the excitation frequency, which is attributed to the aforementioned damped plasma oscillation. From the observed frequency shifts, we estimate  $q_s \approx 12$  using Eq. (5). In contrast to that, the 0 sccm measurement series in Fig. 5b shows that the  $q_s$  of the system without plasma must be so high that no shift of the excitation frequency  $f_x = 2.45$  GHz can be detected.

Another noticeable effect in the EM emission spectra at  $Q = 1$  sccm in Fig. 4 is the EM emission between 30 and 300 MHz. It is clearly detectable inside the SAC test facility as this frequency range is below the lower frequency boundary of the RVC test facility. Additional data sets of the EM emission of the operating ECR thruster in this frequency range are shown in Figs. 6, 7 and 8. It is important to note that these broadband emissions are particularly evident when the max.-peak detector is used. Using an average detector instead may only provide a signal that does not rise significantly above the noise floor. This indicates that these emissions are due to sporadic, semi-continuous effects of the plasma. Even in an gliding arc plasma reactor, which generate arcs that have an inherently intense and broadband EMI, average detector measurements are typically less than one-fourth the amplitude of max-peak measurements in the same frequency range [37].

These emission bands are only measurable if a plasma is burning. Since such behavior could not be detected without a plasma inside the thruster, we attribute these emissions to plasma-related effects. We assume that there is additional emission below 30 MHz, but this is not accessible for us because it is outside the range of our current setup. Similar data on an ECR thruster with a neutralizer generating broadband noise in [8] reveal emissions down to at least 14 kHz. With an excitation power of about 30 W plus 10 W neutralizer, the radiated emissions of [8] may be comparable to our results by assuming a linear downscaling of up to a factor 4 equals 12 dB respectively. Even if subtracting 12 dB from the ordinate, the emissions of that EP system still not fall below our data in most of the frequency range, since that system exhibits broadband emissions that reach higher frequencies. This suggests that linear scaling is not applicable for assessing the magnitude of a DUT's emission at another operating point. Therefore, we believe that the main reason for the difference in emission behavior is the very different topology of the two DUTs. Thus, their emitting behavior cannot be compared directly. Although both thrusters use ECR excitation, ours has a magnetic nozzle instead of a grid system, which requires an additional neutralizer [8]. One possible explanation for our plasma-related emissions are the  $E \times B$  drift instabilities (EDI), which may occur in the 1 – 100 MHz frequency range [38], despite our emissions reaching 300 MHz. Another explanation could be that these emissions may be associated with plasma oscillations, which depend mainly on the electron density of the plasma generated.

Figure 6 shows three EM emission spectra of the ECR thruster operated with the same operational parameters ( $f_x = 2.45$  GHz,  $P_x = 10$  W,  $Q = 1$  sccm Xe), but recorded in three

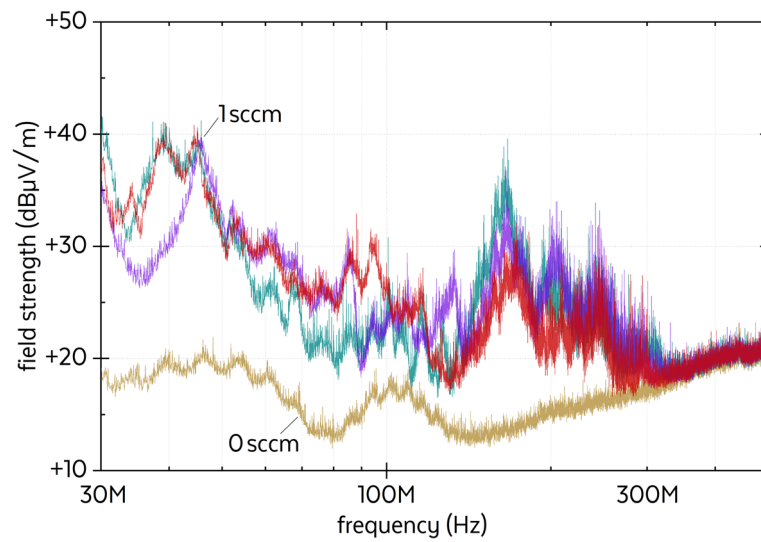


**Fig. 6** Electromagnetic emission spectra of the ECR thruster operated with the same operational parameters ( $f_x = 2.45$  GHz,  $P_x = 10$  W,  $Q = 1$  sccm Xe). The spectra were recorded with the same setup during different measurement campaigns. A reference spectrum recorded without plasma ( $Q = 0$  sccm) is shown for comparison. The spectra are recorded by max.-peak detector at 1 m antenna distance inside the SAC test facility

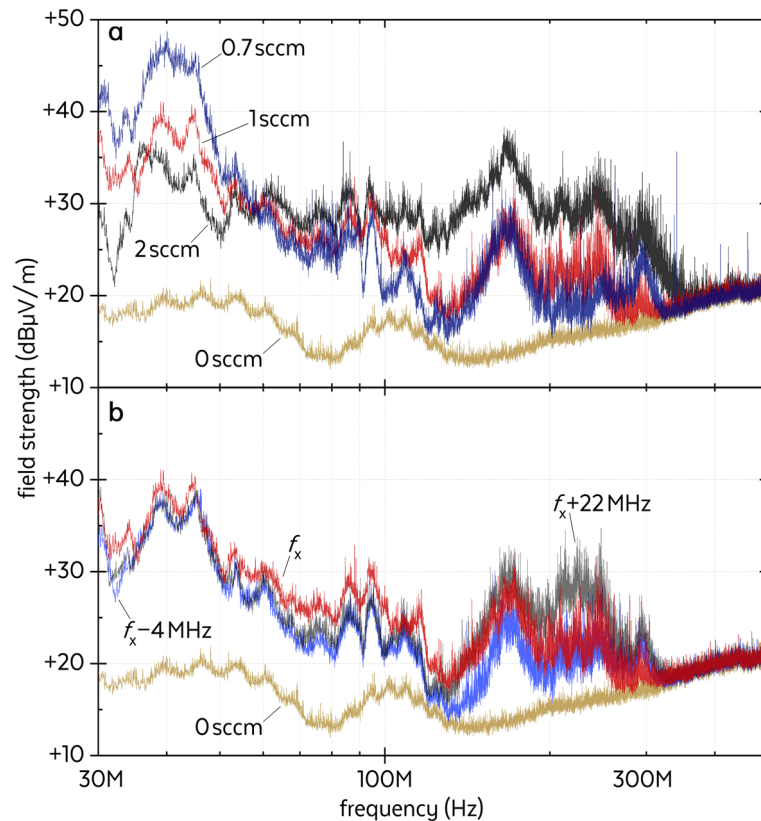


**Fig. 7** Electromagnetic emission spectra of the ECR thruster operated with  $f_x = 2.45$  GHz and  $P_x = 10$  W excitation **a** for various mass flows  $Q$  of xenon propellant and **b** for a variation of  $f_x$  at constant  $P_x$  and constant  $Q = 1$  sccm xenon propellant mass flow. The spectra are measured by max.-peak detector at 1 m antenna distance inside the SAC test facility

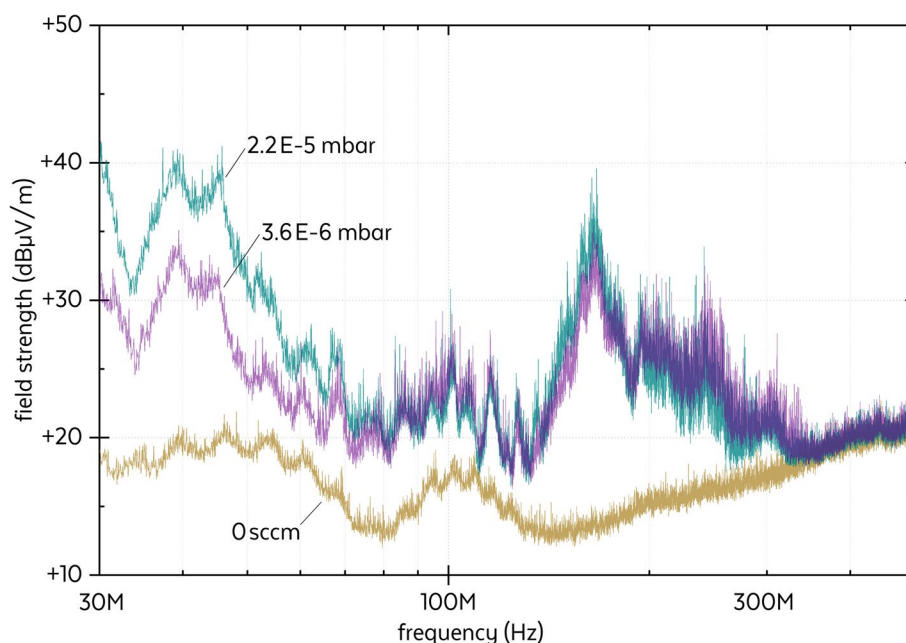


**Fig. 8** Electromagnetic emission spectra of the ECR thruster operated with the same operational parameters ( $f_x = 2.45$  GHz,  $P_x = 10$  W,  $Q = 1$  sccm Xe) for two different background pressures achieved by operating the pumping system without and with an additional cryogenic pump. The spectra are measured by max.-peak detector at 1 m antenna distance inside the SAC test facility

different measurement runs, together with a reference spectrum of the ECR thruster without plasma ( $Q = 0$  sccm). Between the runs, the thruster was dismantled, disassembled and cleaned, reassembled and remounted. To avoid the effects of thermal drift, the thruster fired at its operating point for at least half an hour before starting a measurement, which in turn was performed as quickly as possible. It can be clearly seen that the field strength in the reference spectrum in the frequency range below 300 MHz is always lower than that in the spectra of the operating thruster. Furthermore, the mounting and remounting of the thruster between the measurement runs affects the reproducibility of the measurements, despite an identical setup. The spectra recorded in the three different runs show significant differences in their appearance. The reason are unavoidable small changes in the setup which lead to more or less pronounced changes in the emission characteristics. Observing the average received power would decrease the level of uncertainty [39], but it would not yield results significantly higher than the noise floor. In this case, it is therefore difficult to evaluate individual maxima and minima. Overall, however, it can be stated that the generated plasma leads to broadband emissions in this frequency range. Furthermore, the correction for  $\hat{g}_{\max}$  was omitted because the MIL-STD-461G limits are intended to be checked over reflective ground and shall not be further corrected for ground reflections.

Further evidence that the emissions below 350 MHz are due to plasma-related effects is given by their strong dependence on the operational parameters of the thruster. Figure 7a shows the emission spectra for various propellant mass flows  $Q$  for a given excitation frequency  $f_x = 2.45$  GHz and power  $P_x = 10$  W. Lower values of  $Q$  lead to higher emission amplitudes in the range of lower frequencies below 60 MHz. The situation is

reversed at higher frequencies where the emission bands increase with increasing  $Q$ , in particular in the range between 80 and 300 MHz. However, the dependence on  $Q$  in this higher frequency up to the upper cut-off frequency of about 350 MHz is less pronounced. Changing the excitation power  $P_x$  was only possible in a window of about  $\pm 40\%$  with the chosen setup and had only a small influence on the emission behavior compared to changing  $Q$ . Changing the excitation frequency  $f_x$  also has only a very small influence on the emission behavior compared to  $Q$ . Besides the depicted emission spectra recorded at the nominal operating frequency  $f_x = 2.45$  GHz, the operation at the boundaries of the possible operating frequencies of this ECR thruster, i.e., 2.446 and 2.472 GHz, are shown in Fig. 7b for a constant  $Q = 1$  sccm and constant  $P_x = 10$  W.

As the cryogenic pump was put into service at the end of our measurement campaign, we could study the effect of different background pressures. Corresponding results are presented in Fig. 8. The performance of the ECR thruster depends on background pressure [14], which again seems to have an influence on the plasma-related electromagnetic emission. Below 80 MHz, the magnitude of the emissions rises significantly with increasing pressure. Above 80 MHz, both results differ only slightly. However, from 200 MHz up to the point where the plasma-related effects fall below the noise floor, the emissions at the lower pressure are slightly above the ones measured at higher pressure. An explanation for these findings may be the following: A lower pressure leads to lower propellant gas densities inside the discharge channel and the surrounding chamber, which again may influence the overall particle interactions.

In addition, Fig. 9 shows the influence of measurement angle and antenna polarization on the plasma-related emission of the ECR thruster in the frequency range below 300 MHz. The corresponding series of measurements was recorded while the thruster was operated at  $f_x = 2.45$  GHz,  $P_x = 10$  W, and  $Q = 1$  sccm. The polarized spectra are combined according to Eq. (1) in order to obtain max.-peak emission spectra of the kind shown in Figs. 6, 7 and 8. Figure 9 shows the ECR thrusters orientation and polarization dependent emission in this range. As mentioned earlier and shown in Fig. 6, it is difficult to interpret the shape of individual peaks, for example, because of the limited reproducibility of the emission measurement. Apart from that, if we compare the vertical measurement series, we can see that their shape and amplitude differ only slightly at all measurement angles. In contrast, horizontal polarization emissions tend to increase with measurement angle for this broadband measurement subrange. A reason for the origin of this behavior in horizontal polarization may lie in differences in the electromagnetic visibility for the antenna of different plasma regions, which act as source of the radiated emission. Especially in antenna position  $0^\circ$ , e.g., two supply cables of the thruster (DUT) itself are located between the ion plume and the antenna. These cables may influence the measurements at positions corresponding to lower angles.

## Conclusion

Measurements conducted on an ECR thruster in both a semi-anechoic and reverberation test facility have demonstrated that a plasma inside the operating device functions as a source of electromagnetic radiation causing electromagnetic interference. Specifically, the plasma of the ECR thruster studied is quasi-neutral as it uses a magnetic nozzle

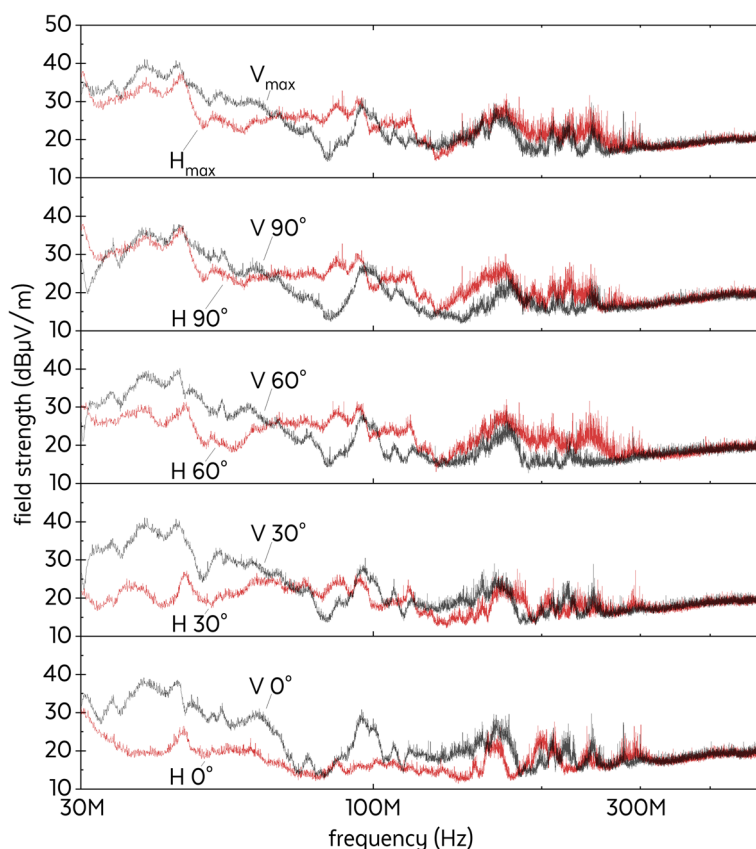


**Fig. 9** Series of the electromagnetic emission spectra of the ECR thruster for horizontal H and vertical V antenna polarization for four different measurement angles. The top graph shows the combination to the maximum values per polarization for  $f_x = 2.45$  GHz and  $P_x = 10$  W excitation at  $Q = 1$  sccm xenon propellant mass flow, measured by max.-peak detector at 1 m antenna distance in the SAC test facility

for plume extraction. This is advantageous as it eliminates the need for an external neutralizer, which can cause additional interference in the emission measurement.

A vacuum-accessible SAC is suitable for broadband studies, particularly at the lower frequency limit for radiated emission measurements, as per the MIL standard, respectively at 30 MHz in our case. Conversely, the RVC approach is better suited for higher frequency investigations because of its system gain that may provide a lower noise floor, especially when studying DUTs that are periodic emitters. However, it has a low cutoff frequency that limits its usage at frequencies below 500 MHz. Nonlinearities in all noise plots primarily result from correction tables and attenuation settings associated with the chosen setup. Moreover, one should estimate setup effects such as floor reflections or material properties of the vacuum system since they may affect the measurements adopted by the standard. Despite different measurement principles, both facilities yield comparable results in the usable frequency range of 500 MHz to 18 GHz in our case. It should be noted that small changes in the setup may lead to significant variations in the measured emission results.

Radiated emissions from a device under test occur as a combination of effects attributable to the plasma and its excitation-related effects, e.g. during signal generation and transmission. Plasma-related emissions can occur in various frequency ranges,

depending on the plasma excitation process utilized—in our study, electron cyclotron resonance excitation. We observed broadband electromagnetic emissions approximately a decade below the excitation frequency and even lower. The emissions' amplitude and shape depend mainly on the mass flow of the propellant, rather than the frequency or power of the excitation. An explanation of the broadband plasma related emissions could lie in the  $E \times B$  electron drift instabilities [38] or plasma oscillations, depending primarily on the electron density of the plasma.

Another plasma effect becomes apparent in the vicinity of the excitation frequency. Electron oscillations are stimulated not only at the excitation frequency but also within a narrow range around this frequency, lying primarily below the excitation frequency peak reflecting the quality factor of the thruster with ignited plasma as a resonator. Harmonics of this frequency can be observed in the emission spectrum, too, but their origin appears to be a generator effect rather than plasma induced. As for the plasma emission directivity, there is no significant polarization or orientation dependence in terms of field strength. Since the ECR thruster can be regarded as a radio-technical device, exceeding the limit values for the operating frequency and its harmonics is permissible. This means that the thruster emission behavior in the measured frequency range at the operational points studied is below the limit set by the ECSS-E-ST-20-07C standard.

## Nomenclature

$f_x$  excitation frequency of the ECR thruster

$P_x$  input power of the excitation frequency of the ECR thruster

$P_{f-r}$  same as  $P_x$  when neglecting metering errors through cable losses

$Q$  mass flow of xenon propellant inlet of the ECR thruster

$A(f)$  amplitude spectra of e.g. electromagnetic emission

$g_{\max,H}(f)$  estimated influence through ground reflections on horizontal polarized waves in SAC

$\hat{g}_{\max}(f)$  estimated maximum influence through ground reflections in SAC

$f_{\min}$  lowest working frequency of the RVC to comply EMC requirements

$A_c$  total cable attenuation in dB of the feed line section between directional coupler and thruster

$q_s$  quality of a damped oscillator system, here the ECR thruster

## Acknowledgements

We would like to thank the Center of Competence for Nanotechnology and Photonics of the THM—University of Applied Sciences in Gießen, which supported the design of the semi-anechoic chamber and financed part of the measurement equipment and software. We would also like to thank ONERA, on the one hand, for lending us the ECR thruster developed in the MINOTOR project and, on the other hand, for granting permission to publish the results of the EMC measurements.

## Code availability

Measurements were performed using Rohde & Schwarz' software EMC32 on version 11.40.00.

## Authors' contributions

F. Kiefer conducted measurements and drafted the manuscript. K. Keil conducted measurements and characterized the plasma. K. Holste and R. Thueringer discussed the data and supported the project organization. P. J. Klar provided facilities and equipment and supervised the project. ONERA has granted approval for the utilization of the DUT and has authorized the publication of our investigation outcome. All authors read and approved it.

## Funding

Open Access funding enabled and organized by Projekt DEAL. This project is supported by funds of "Bundesministerium für Bildung und Forschung" (BMBF) under grant no 13FH173PX8, "Bundesministerium für Wirtschaft und Energie" (BMWi) under grant no 50RS1903 and EU regional funding via the EFRE scheme of the State of Hesse.

**Availability of data and materials**

Data available from F. Kiefer upon reasonable request and subject to ONERA's permission.

**Declarations****Competing interests**

The authors declare no competing interests.

Received: 13 December 2023 Accepted: 8 April 2024

Published: 2 May 2024

**References**

1. Denis G et al (2020) From new space to big space: How commercial space dream is becoming a reality. *Acta Astronaut* 166:431–443. <https://doi.org/10.1016/j.actaastro.2019.08.031>
2. Holste K et al (2020) Ion thrusters for electric propulsion: Scientific issues developing a niche technology into a game changer. *Rev Sci Instrum* 91:061101. <https://doi.org/10.1063/5.0010134>
3. Kodheli O et al (2021) Satellite communications in the new space era: a survey and future challenges. *IEEE Commun Surv Tutor* 23(1):70–109. <https://doi.org/10.1109/COMST.2020.3028247>
4. Chrysaki M (2020) The sustainable commercialisation of space: the case for a voluntary code of conduct for the space industry. *Space Policy* 52:101375. <https://doi.org/10.1016/j.spacepol.2020.101375>
5. Curzi G, Modenini D, Tortora P (2020) Large constellations of small satellites: a survey of near future challenges and missions. *Aerospace* 07(9):133. <https://doi.org/10.3390/aerospace7090133>
6. Ciccolella A, Marliani F (2009) EMC in space systems: current practices and future needs - The ESA perspective. *URSI Radio Sci Bull.* 328:9–19. <https://doi.org/10.23919/URSIIRSB.2009.7909537>
7. Zhang H et al (2020) *Spacecraft Electromagnetic Compatibility Technologies*. Beijing Institute of Technology Press and Springer Nature Singapore Pte Ltd, Singapore, p 65 473–474. <https://doi.org/10.1007/978-981-15-4782-9>
8. Nishiyama K et al (2007) Ground chamber measurements of the electromagnetic emissions from the Hayabusa ion engine. *J Propuls Power* 23(3):513–521. <https://doi.org/10.2514/1.19473>
9. Bogorod AL et al (2008) Radiated emissions and magnetic field characterization of a 2-kW electrothermal propulsion system. *IEEE Trans Electromagn Compat* 50(3):466–475. <https://doi.org/10.1109/TEMC.2008.927941>
10. Correyero S, Jarrige J, Packan D, Ahedo E (2019) Plasma beam characterization along the magnetic nozzle of an ECR thruster. *Plasma Sources Sci Technol* 28:095004. <https://doi.org/10.1088/1361-6595/ab38e1>
11. Correyero S, Merino M, Elias P-Q, Jarrige J, Packan D, Ahedo E (2019) Characterization of diamagnetism inside an ECR thruster with a diamagnetic loop. *Phys Plasmas* 26:053511. <https://doi.org/10.1063/1.5093980>
12. Sánchez-Villar A et al (2021) Coupled plasma transport and electromagnetic wave simulation of an ECR thruster. *Plasma Sources Sci Technol* 30:045005. <https://doi.org/10.1088/1361-6595/ab38e1>
13. Sánchez-Villar A et al (2023) Comparison of a hybrid model and experimental measurements for a dielectric-coated coaxial ECR thruster. *Plasma Sources Sci Technol* 32:014002. <https://doi.org/10.1088/1361-6595/acb00c>
14. Désangles V et al (2023) ECRA thruster advances: 30W and 200W prototypes latest performances. *J Electr Propuls* 2:10. <https://doi.org/10.1007/s44205-023-00046-x>
15. Kiefer F, Holste K, Klar PJ et al (2023) Reverberation chamber for electromagnetic compatibility testing of electric thrusters. *J Electr Propuls* 2:9. <https://doi.org/10.1007/s44205-023-00038-x>
16. Rover Y, Thüringer R, Volkmar C et al (2023) Semi-anechoic chamber for electromagnetic compatibility tests of electric propulsion thrusters. *J Elec Propuls* 2:3. <https://doi.org/10.1007/s44205-023-00039-w>
17. Interface Standard (2015) MIL-STD-461G: Requirements for the control of electromagnetic interference characteristics of subsystems and equipment. Department of Defense, USA
18. European Cooperation for Space Standardization (2012) ECSS-E-ST-20-07C Rev. 1: Space engineering – Electromagnetic compatibility. ECSS Secretariat ESA-ESTEC, Noordwijk
19. Beiting EJ, Garret ML (2012) Facility for high-fidelity electromagnetic compatibility studies of electric thrusters. *AIAA* 2007–5329. <https://doi.org/10.2514/6.2007-5329>
20. Beiting EJ (2012) Design and performance of a facility to measure electromagnetic emissions from electric satellite thrusters. *AIAA-2001–3344*. <https://doi.org/10.2514/6.2001-3344>
21. Albani M et al (2018) High-frequency characterization of EMI/EMC ground test facility for the measurements of electric propulsion thruster emissions. 12th European Conference on Antennas and Propagation (EuCAP 2018). <https://doi.org/10.1049/cp.2018.1048>
22. Albani M et al (2017) Modeling and dielectric characterization of EMI/EMC ground test for the evaluation of the electric propulsion thruster emissions. 2017 IEEE International Symposium on Antennas and Propagation & USNC/URSI National Radio Science Meeting, pp. 2599–2600. <https://doi.org/10.1109/APUSNCURSINRSM.2017.8073342>
23. Plokhikh AP, Vazhenin NA, Merkurev DV (2023) Propellant influence on electromagnetic environment generated by stationary plasma thrusters. *Cosmic Res* 61(5):396–403. <https://doi.org/10.1134/S0010952523700375>
24. Plokhikh AP et al (2022) Spectral characteristics of self-emission from electric thrusters with closed electron drift in the radio-frequency band for various propellants. *Cosmic Res* 60(5):405–411. <https://doi.org/10.1134/S0010952522050069>
25. Plokhikh AP, Vazhenin NA, Popov GA (2019) Analysis of the influence of electromagnetic emission from stationary plasma thrusters on the interference immunity of the earth-spacecraft communication channel. *Cosmic Res* 57(5):317–324. <https://doi.org/10.1134/S0010952519050071>
26. Baranov SV et al (2018) Electromagnetic emission from electric propulsions under ground conditions. *Therm Eng* 64(13):959–970. <https://doi.org/10.1134/S0040601517130043>

27. Doerner R, White D, Goebel DM (2003) Sputtering yield measurements during low energy xenon plasma bombardment. *J Appl Phys* 93(9):5816–5823. <https://doi.org/10.1063/1.1566474>
28. Kenmotsu T et al (2009) Enhanced sputtering yields of carbon due to accumulation of low-energy Xe ions. *Nucl Instrum Methods Phys Res, Sec B* 267:1717–1720. <https://doi.org/10.1016/j.nimb.2009.01.127>
29. Scharmann S et al (2022) Thrust measurement of an ion thruster by a force probe approach and comparison to a thrust balance. *AIP Adv* 12:045218. <https://doi.org/10.1063/5.0066401>
30. Lobbia RB, Beal BE (2017) Recommended practice for use of langmuir probes in electric propulsion testing. *J Propuls Power* 33:3. <https://doi.org/10.2514/1.B35531>
31. Detlefsen J, Siart U (2012) *Grundlagen der Hochfrequenztechnik* 4th edn. Oldenbourg Wissenschaftsverlag GmbH, Munich, pp 231–234. <https://doi.org/10.1524/9783486716238>
32. Nikolopoulos CD (2021) Recent trends on electromagnetic environmental effects for aeronautics and space applications. IGI Global, Hershey, p 107. <https://doi.org/10.4018/978-1-7998-4879-0>
33. NASA Technical Standard (2013) MSFC-SPEC-521C: electromagnetic compatibility requirements for equipment and subsystems. Marshall Space Flight Center, Alabama, p 35812
34. NASA Technical Standard (2013) GSFC-STD-7000A: general environmental verification standard. Goddard Space Flight Center, Maryland, p 20771
35. Industrial Technote (2010) AN-106 AF: Use of Antenna Factors in EMI Measurements. Com-Power Corporation, Silverado. (last checked: 2024-02-20) [https://www.com-power.com/uploads/technote/AN-106\\_Antenna\\_Factor.pdf](https://www.com-power.com/uploads/technote/AN-106_Antenna_Factor.pdf)
36. Tipler PA, Mosca G (2019) *Physik*, 8th edn. Springer Spektrum, Berlin, p 450. <https://doi.org/10.1007/978-3-662-58281-7>
37. Mazurek P (2020) Chosen aspects of the electromagnetic compatibility of plasma reactors with gliding arc discharges. *Appl Sci* 10:3789. <https://doi.org/10.3390/app10113789>
38. Mazière V et al (2022) Broadband (kHz–GHz) characterization of instabilities in Hall thruster inside a metallic vacuum chamber. *Phys Plasmas* 29:072107. <https://doi.org/10.1063/5.0090774>
39. Boyes SJ, Huang Y (2016) *Reverberation chambers – theory and applications to EMC and antenna measurements*. Wiley, Chichester, p 120. <https://doi.org/10.1002/9781118906279>